Copyright Notice

Energetically Optimal Path Following for Electric Aircraft Taxi Systems Based on Convex Optimization

Fabrizio Re*, Ricardo de Castro†
DLR German Aerospace Center
Institute of System Dynamics and Control
Oberpfaffenhofen, Germany
Email: *fabrizio.re@dlr.de, †ricardo.decastro@dlr.de

***Abstract*—In an effort to reduce aircraft fuel consumption and emissions in airports, electric driving systems are being studied by several stakeholders. When assessing the overall benefit at mission level in the design of those systems, it is necessary to determine the optimal control strategy of the system on ground for a given architecture in order to compare the performances of different designs. This paper deals with optimal path-following of taxi trajectories with an aircraft equipped with a specific architecture of electric driving system. The problem is formulated in convex form to ensure that a global optimum is found. While different objectives may be pursued, the most important one for this application is the minimization of the fuel consumption of the Auxiliary Power Unit (APU) that supplies the electric driving system. Critical system constraints such as the thermal behavior of the electric motors are considered. Finally, results of several optimization setups with different objectives and constraints are presented and compared.**

I. Introduction

Several recent research projects have been studying low- or zero-emission ground propulsion technologies with the aim of decreasing the fuel consumption and emissions of commercial flights during taxi phases in airports [1]–[5]. Conventional aircraft move on ground by means of the idle thrust of the main jet engines, which are extremely inefficient in this operating condition. Moreover, the emissions contain a high amount of polluting agents like carbon monoxide (CO) due to incomplete fuel combustion [6]. Idling jet engines also generate a large amount of the noise in airport areas. Finally, the idle thrust is often too large and makes it necessary to pulse the brakes periodically to maintain a steady speed, which results in unnecessary heat generation and wear on the braking system. While these drawbacks have been considered somewhat unavoidable throughout the history of aviation, an interest has grown in the last years in exploiting the saving potential of the taxi phases. Efforts are particularly concentrated on fitting electric motors into the main landing gear, which appears to be the most viable layout for a low-emission system [7]. The power source would be the Auxiliary Power Unit (APU). This is the on-board jet engine generator that, on today's conventional aircraft, provides power for starting up the main jet engines as well as electric, hydraulic, and pneumatic power to the aircraft systems when the main engines are off. Being designed for a maximum power of some hundred kilowatts on a narrow-body aircraft, its efficiency can be expected to be much higher than the main engines running at idle. Moreover, if taxi is performed without main engines, the APU needs to be running to supply power to the avionic systems, hence it would also be available as power supply for the electric driving system at little additional cost. Designing such an electric taxi system presents two main challenges. First, integration of the electric drivetrain in the landing gear assembly is an issue, as there is very limited available room in current landing gear designs and the environmental conditions are very harsh, needing a high degree of protection and mechanical robustness. Second, a new system adds additional weight to the aircraft, resulting in a lower efficiency in flight and possibly even worsening the overall balance of a whole gate-to-gate mission. Trade-offs are needed on different aspects. The system must be as lightweight as possible to minimize the performance loss in flight, while being still powerful enough to offer a sufficient performance for taxi operation. The best design for a given aircraft architecture will strongly depend on the profile and length of the missions typically flown with that aircraft. Also, it is necessary to push the electric system to its operational limits to maximize the benefit. Most notably, the thermal behavior of the electric motors is key: the operational envelope must be exploited fully, which in turn influences the motor design and its control along the taxi path.

In the framework of the design of an electric aircraft taxi system, this work presents an optimization strategy for the path-following of assigned taxi trajectories with a mid-size, narrow-body aircraft equipped with two electric motors on the main landing gears. Particular attention will be given to the convexification of this optimization problem [12], which allows us to obtain globally optimal solutions for a given taxi system, trajectory and aircraft type. The result of this optimization can be used in the performance assessment of selected architectures during the design process. Starting from the convex formulations of minimum-time path following problems studied in robotics and vehicle dynamics [10], [11], we adapt those formulations to the present problem. To keep the problem tractable, a simple dynamic model will be used. While time optimality and performance maximization are common goals in robotics and vehicle dynamics problems, the most important optimization objective in this case is the energy minimization in order to maximize the benefit of the taxi system. Other constraints such as thermal behaviour and speed and power limits along the trajectory are also considered.

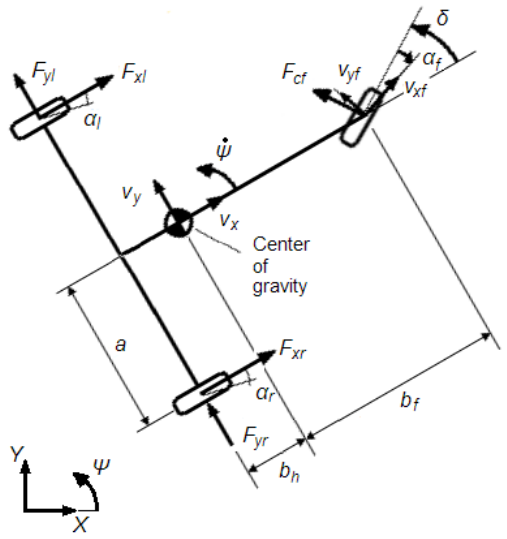

Fig. 1. Model of an aircraft on ground

II. Vehicle Dynamic Model

The equations of motion of the aircraft on ground are derived from the vehicle illustrated in Fig. 1. The model features one wheel per landing gear. Each main gear wheel is assumed to be connected to one electric motor capable of providing both a driving and a braking moment. The nose gear wheel is steerable and spins freely, i.e. its axial moment is assumed zero. Vertical dynamics, roll and pitch, and the main jet engines are neglected. In addition, pure rolling is assumed for all wheels since moderate driving and braking forces are considered compared to the vehicle mass.

The equations of motion in the local (vehicle's) reference frame are:

$$m\left(\dot{v}_x - \dot{\psi} v_y\right) = F_x = -F_{cf}\sin\delta + \frac{(T_l + T_r)}{R_R} - F_r \quad (1)$$

$$m\left(\dot{v}_y + \dot{\psi} v_x\right) = F_y = F_{yl} + F_{yr} + F_{cf}\cos\delta \quad (2)$$

$$J_z\ddot{\psi} = M_z = b_f F_{cf}\cos\delta + \frac{a\,(-T_l + T_r)}{R_R} - b_h\,(F_{yl} + F_{yr}) \quad (3)$$

where v_x is the longitudinal speed; v_y is the lateral speed; $\dot{\psi}$ is the yaw angle, m is the vehicle mass; J_z is the vehicle moment of inertia around the yaw axis; δ is the nose gear steering angle; $F_{cf} = f(v_x, \dot{\psi}, \delta)$ is the cornering force of the nose gear wheel; R_R is the effective radius of the main gear wheels; T_l and T_r are the torques applied on the wheel of the left and right main gear respectively; F_r is a term subsuming all the resistances; a, b_f, and b_h are geometric parameters that characterize the position of the centre of gravity as shown in Fig. 1. In the present problem, the resistance F_r is considered constant as the only considerable resistance is the tire rolling friction, which can be modeled as a function of the mass scaled by a constant rolling friction coefficient μ_R.

The cornering forces of the tires F_{cf}, F_{yl}, F_{yr} are functions of their sideslip angles $\alpha_f, \alpha_l, \alpha_r$, which in turn depend on the vehicle kinematics as follows:

$$\alpha_f = \delta - \arctan\frac{v_y + b_v\dot{\psi}}{v_x} \quad (4)$$

$$\alpha_l = -\arctan\frac{v_y - b_h\dot{\psi}}{v_x - a\dot{\psi}} \qquad \alpha_r = -\arctan\frac{v_y - b_h\dot{\psi}}{v_x + a\dot{\psi}} \quad (5)$$

We assume the tire lateral forces to be a linear function of the sideslip multiplied by the cornering stiffness c_f, c_r (for front and rear tires respectively) until reaching the saturation forces $F_{yf,max}, F_{yl,max}, F_{yr,max}$ which are modeled as constants. For the rear tires:

$$F_{yi} = \begin{cases} F_{yi,max}\cdot\operatorname{sign}(c_r\alpha_i) & \text{if} c_r\alpha_i \geq F_{yi,max} \\ c_r\alpha_i & \text{otherwise} \end{cases} \quad (6)$$

with $i = \{l, r\}$. The same holds for the front tire by considering the index cf.

The vehicle trajectory is described through the time functions of the X-position, Y-position and course (i.e. yaw angle) in the global coordinate system fixed with the ground surface as follows:

$$\mathbf{p}(t) = [p_X(t) \quad p_Y(t) \quad p_\psi(t)] \quad (7)$$

In defining the trajectory, the sideslip angle $\beta = \arctan(v_y/v_x)$ is set to zero at all times. This is done by requiring that the course be tangent to the trajectory arc at all times. The zero sideslip angle condition directly results in $v_y = 0 \;\forall\; v_x \neq 0$.

We now introduce the transformation matrix $\mathbf{T}(\mathbf{p})$ from the global to the local coordinate system as function of the trajectory presented in (7):

$$\mathbf{T}(\mathbf{p}) = \begin{bmatrix} \cos p_\psi & \sin p_\psi & 0 \\ \sin p_\psi & -\cos p_\psi & 0 \\ 0 & 0 & 1 \end{bmatrix} \quad (8)$$

The vehicle dynamic equations (1), (2), and (3) can be transcribed into global coordinates:

$$\mathbf{M}\ddot{\mathbf{p}} = \mathbf{T}(\mathbf{p})\,(\mathbf{F} - \mathbf{R}) \quad (9)$$

where the matrix $\mathbf{M}$ is composed as follows:

$$\mathbf{M} = \begin{bmatrix} m & 0 & 0 \\ 0 & m & 0 \\ 0 & 0 & J_z \end{bmatrix}$$

and the vectors $\mathbf{F}$ and $\mathbf{R}$ summarize the forces and the resistances of the dynamic equations in the local frame:

$$\mathbf{F} = \begin{bmatrix} F_x \\ F_y \\ M_z \end{bmatrix} \qquad \mathbf{R} = \begin{bmatrix} F_r \\ 0 \\ 0 \end{bmatrix} \quad (10)$$

The electric motors fitted on each main landing gears can produce a positive (driving) or a negative (braking) torque T_r resp. T_l. We consider ideal motor models with bounded torque and power as follows:

$$-T_{max} \leq T_i(t) \leq T_{max} \quad (11)$$

$$P_{max} \leq T_i(t)\omega_i \leq P_{max} \quad (12)$$

with the index $i = \{l, r\}$ standing respectively for left (T_l, ω_l) and right motor (T_r, ω_r).

In addition, a simplified thermal behavior of the motors is considered. While a detailed modeling of the temperature field and cooling behavior of the electric motors is clearly necessary when designing the new driving technology, its incorporation into the optimization problem becomes cumbersome. To address this issue, we assume that for a given motor, the most critical point with regard to temperature is known in advance. This point is subject to a heating power proportional to the square of the motor current, which is taken equal to the square of the motor torque neglecting any secondary effects such as inductance or saturation, and a cooling power dependent on the temperature. The nature of the cooling is not further investigated here, although it will be a combination of conduction and convection in reality. The temperature obeys a basic differential equation of the following type:

$$\dot{\theta}_i(t) = k_h T_i^2(t) - k_c\left(\theta_i(t) - \theta_{amb}\right) \quad \text{with } i = l, r \tag{13}$$

with $\theta_i(t)$ critic temperature, i.e. the temperature at the critical point of one motor; θ_{amb} ambient temperature; k_h and k_c appropriate heating resp. cooling coefficients.

Regarding the energy consumption of the vehicle, the following assumptions are made. First, there is no energy storage device allowing regenerative braking; therefore the power generated when braking is not stored and considered lost (i.e. converted into heat as in rheostatic braking). The added benefit of those devices will be investigated in future works. Second, the driving power is drawn from the APU. Based on the data in [9], its fuel consumption can be modeled as a linear function of the total driving power demand. Any losses in the inverters controlling the motors are neglected, thus it is assumed that the total power equals the sum of the driving powers of the two motors. The APU fuel flow c is then:

$$c = c_0 + c_1\left[\max(0, T_l(t))\omega_l(t) + \max(0, T_r(t))\omega_r(t)\right] \tag{14}$$

with c_0 fuel flow at idle, c_1 additional fuel flow per unit of generated power, ω_l and ω_r rotational speeds of the motors.

III. Setup of the convex optimization problem

A. Equations of Motion

This section presents the formulation of the path-following optimization problem for the aircraft during the taxi phase. Toward that goal, we will follow closely the convex optimization methodology introduced in [10] in a robotic context and applied in [11] in a vehicle dynamics problem. The starting point consists in using the path s along the trajectory as independent variable instead of the time. The travel time t at any point s along the trajectory is as follows:

$$\dot{s} = \frac{ds}{dt} \quad \Rightarrow \quad t = \int_s dt = \int_0^s \frac{1}{\dot{s}} ds \tag{15}$$

This allows us to describe $\mathbf{p}(s)$ and its first and second time derivative as

$$\begin{aligned} \dot{\mathbf{p}}(s) &= \mathbf{p}'(s)\,\dot{s} \\ \ddot{\mathbf{p}}(s) &= \mathbf{p}''(s)\,\dot{s}^2 + \mathbf{p}'(s)\,\ddot{s} \end{aligned} \tag{16}$$

Next, introducing the following change of variables:

$$a(s) = \ddot{s}, \qquad b(s) = \dot{s}^2,\ b > 0 \tag{17}$$

enables us to rewrite (9) as an affine relationship of $a(s)$, $b(s)$, $T_l(s)$, $T_r(s)$, $F_{yf}(s)$ and a linear differential equation coupling a and b:

$$a(s) = \frac{d\dot{s}}{dt} = \dot{s}\frac{d\dot{s}}{ds} = \frac{1}{2}\frac{d\dot{s}^2}{ds} = \frac{1}{2}\frac{db(s)}{ds} \tag{18}$$

$$\mathbf{m}(\mathbf{s})a(s) + \mathbf{r}(\mathbf{s})b(s) = \mathbf{F}(\mathbf{s}) - \mathbf{R} \tag{19}$$

$$\begin{aligned} \mathbf{m}(s) &= \mathbf{T^{-1}}(\mathbf{p}(\mathbf{s}))\ \mathbf{M}\ \mathbf{p}'(\mathbf{s}) \\ \mathbf{r}(s) &= \mathbf{T^{-1}}(\mathbf{p}(\mathbf{s}))\ \mathbf{M}\ \mathbf{p}''(\mathbf{s}) \end{aligned}$$

representing linear (and convex) constraints.

B. Center of Gravity Forces

In order to tackle the tire lateral forces, it is necessary to deal with the tire sideslips. Inspecting (5), one can find that the sideslip angles of the main gear wheels are dependent on the local speed vector $\mathbf{v}$, which is a function of the path s and its first time derivative $\dot{s}$:

$$\mathbf{v} = \begin{bmatrix} v_x \\ v_y \\ \psi \end{bmatrix} = \mathbf{T}^{-1}(\mathbf{p}(s))\ \mathbf{p}'(s)\dot{s} = \begin{bmatrix} L_x(s) \\ L_y(s) \\ L_{\psi}(s) \end{bmatrix} \dot{s} \tag{20}$$

where we introduced $L_x(s), L_y(s), L_{\psi}(s)$ as the components of the product $\mathbf{T}^{-1}(\mathbf{p}(s))\ \mathbf{p}'(s)$. Substituting the speeds in (5), we obtain:

$$\alpha_l = \arctan\frac{L_y - b_h L_{\psi}}{L_x - aL_{\psi}}\frac{\dot{s}}{\dot{s}} \qquad \alpha_r = \arctan\frac{L_y - b_h L_{\psi}}{L_x + aL_{\psi}}\frac{\dot{s}}{\dot{s}}$$

and canceling the occurrences of $\dot{s}$:

$$\alpha_l = \arctan\frac{L_y(s) - b_h L_{\psi}(s)}{L_x(s) - aL_{\psi}(s)} \tag{21}$$

$$\alpha_r = \arctan\frac{L_y(s) - b_h L_{\psi}(s)}{L_x(s) + aL_{\psi}(s)} \tag{22}$$

This shows that the sideslip angles of the main gear (rear axle) are only dependent on the position s along the path. This function is known in advance once the trajectory is fixed. When defining the trajectory and calculating the main gear tire forces, the tire saturation limits can be taken into account by bounds $F_{yl,max}, F_{yr,max}$ on the latter.

Considering the vehicle dynamic equations (1), (2), and (3), we rename the y-component of the nose gear wheel force (i.e., lateral force of the front axle) as:

$$F_{yf} = F_{cf}\cos\delta$$

Furthermore, we assume the contribution of the nose gear wheel to the longitudinal motion in (1) as negligible.

The components of the dynamic vector $\mathbf{F}$ can be then written as functions of the path:

$$F_x(s) = \frac{1}{R_R}\left(T_l + T_r\right) - F_r \tag{23}$$

$$F_y(s) = F_{yf} + F_{yl}(s) + F_{yr}(s) \tag{24}$$

$$M_z(s) = b_f F_{yf} + \frac{a\left(-T_l + T_r\right)}{R_R} - b_h\left(F_{yl} + F_{yr}\right) \tag{25}$$

In this way, $F_x(s)$, $F_y(s)$, and $M_z(s)$ are affine functions of $F_{yl}(s)$, $F_{yr}(s)$ as well as $T_l(s)$, $T_r(s)$ and $F_{yf}(s)$ which

are the effects of the three vehicle actuators controlling the motion: two electric motors and nose gear steering system. In the following, we will treat the actuator effects as the three control variables of the problem. In reality however, the controlled variables are some electric quantities (e.g. current) for the motors and the steering angle for the nose gear lateral force. By exploiting knowledge of the system properties, these quantities can be mapped easily to the three dynamic variables used in this problem. In particular for the nose gear, an inverse tire model can be used to calculate the needed steering angle as a function of the required lateral force in dependence of the aircraft speeds. The variable F_{yf} is bounded by a $F_{yf,max}$ corresponding to the maximum tire lateral force. Since safety is of uttermost importance in our application, $F_{yf,max}$ is chosen sensibly lower than the maximum tire lateral force.

C. Power and Thermal Constraints

Reminding that the lateral speed v_y of the vehicle is always assumed to be zero, it follows that $v_x = \dot{s} = \sqrt{b}$. We neglect the effect of the yaw motion on the rotational speed of the main gear wheels, which therefore becomes:

$$\omega_l \approx \omega_r \approx \frac{v_x}{R_R} = \frac{\sqrt{b(s)}}{R_R} \tag{26}$$

The power bound on each motor in (12) becomes:

$$\left| \frac{T_i(s)\sqrt{b(s)}}{R_R} \right| \leq P_{max} \quad \text{with } i = \{l, r\} \tag{27}$$

This function is not convex on T_i and b. The power limitation is therefore approximated through the following linear inequality in T_i and $b(s)$:

$$T_i(s) <= T_{max} - k_P(b(s) - b_P) \quad \text{with } i = \{l, r\} \tag{28}$$

where b_P and k_P are constants determining the position of the power peak and its decrease with growing speed.

The thermal equation (13) can also be rewritten as a function of the independent variable s:

$$\frac{d\theta}{ds}\frac{1}{\sqrt{b}} = \frac{1}{\sqrt{b}}\left[k_h T_i^2(s) - k_c\left(\theta_i(s) - \theta_{amb}\right)\right]$$

Integrating this expression leads to a function that is not convex in the cooling part. For this reason, a temperature limit cannot be set in the convex problem. Instead, a limit on the heating energy over the whole trajectory is set in the following form:

$$\int_0^{\bar{s}} \frac{T_i^2(s)}{\sqrt{b(s)}}\, ds \leq E_{h,max} \quad \text{with } i = \{l, r\} \tag{29}$$

with $E_{h,max}$ maximum allowed heating energy level for each motor over the whole trajectory. Note that $E_{h,max}$ is not an explicit energy, but rather a parameter proportional to the heating energy since no heating coefficients appear in (29). Setting this limit properly for a real application requires knowledge of the real system. (29) is convex as the argument of the integral is convex in T_i and b and the integral preserves the convexity property [12]. This formulation is more conservative than a temperature limit as it neglects the motor cooling.

D. Cost Function and Final Formulation

We consider two different cost functions of the optimization problem depending on the optimization goal. Time minimization is based on the following cost function (using (15)):

$$C_T = \int_0^{t(\bar{s})} t\ dt = \int_0^{\bar{s}} \frac{1}{\dot{s}} ds = \int_0^{\bar{s}} \frac{1}{\sqrt{b(s)}} ds \tag{30}$$

which is convex in b.

The second cost function for fuel consumption minimization is the overall fuel consumption C from $s = 0$ to the end point $\bar{s}$:

$$C_F = \int_0^{t(\bar{s})} c(t) dt \tag{31}$$

Using (15), observing that $\dot{s} = \sqrt{b(s)}$ and reminding the assumptions on the motor speeds in eq. 26, the fuel consumption can be rewritten as a function of s:

$$C_F = \int_0^{\bar{s}} \left[c_0 + \frac{c_1}{R_R}\left(T_l^+(s) + T_r^+(s)\right)\sqrt{b(s)}\right] \frac{1}{\sqrt{b(s)}} ds$$

$$C_F = c_0 C_T + \int_0^{\bar{s}} \left[\frac{c_1}{R_R}\left(T_l^+(s) + T_r^+(s)\right)\right] ds \tag{32}$$

where the shorthand notation $T_i^+ = \max(0, T_i)$ with $i = \{l, r\}$ was used. Note that (32) is convex in b, T_l and T_r. Also, note that the part pertaining to the idle consumption is ultimately C_T weighted by the idle fuel consumption c_0. This suggests that minimizing C_F will result in a trade-off between time minimization (which requires higher average speeds) and energy minimization (which determines lower average speeds).

In summary, the convex optimal path-following problem is:

$$\begin{aligned}
\underset{a,b,T_l,T_r,F_{yf}}{\text{minimize}}\ & \epsilon\, C_T + (1-\epsilon)\, C_F \\
\text{s.t. } & \mathbf{m}(\mathbf{s})a(s) + \mathbf{r}(\mathbf{s})b(s) = \mathbf{F}(\mathbf{s}) - \mathbf{R} \\
& -T_{max} \leq T_i \leq T_{max} \\
& |T_i(s)| <= T_{max} - k_P(b(s) - b_P) \quad i = \{l, r\} \\
& \int_0^{\bar{s}} \frac{T_i^2(s)}{\sqrt{b(s)}}\, ds \leq E_{h,max} \quad i = l, r \\
& -F_{yf,max} \leq F_{yf} \leq F_{yf,max} \\
& a(s) = \frac{1}{2}\frac{db(s)}{ds} \\
& b(s) > 0,\ b(0) = b_0,\ b(\bar{s}) = b_{\bar{s}}
\end{aligned} \tag{33}$$

where the factor ϵ allows us to weigh the relative contribution of each cost function.

Speed limits along the trajectory (e.g. maximum allowed speeds on certain corners) can be included by adding the following constraint to the optimization problem:

$$b(s) <= \bar{v}_x^2(s) \tag{34}$$

where $\bar{v}_x(s)$ is the speed limit along the trajectory.

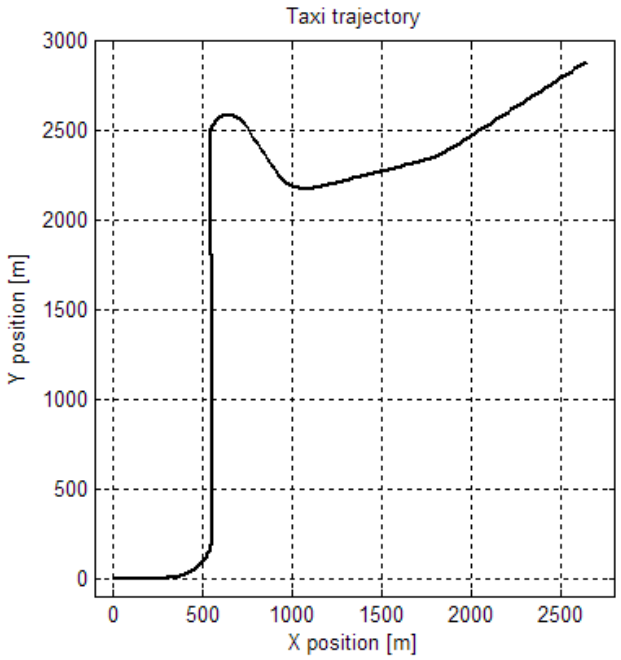

Fig. 2. Trajectory chosen for optimization

IV. Optimization Results

Upon implementation, the optimization problem was transformed into a discrete problem following the collocation method [13], in which the dynamic equations are discretized by the trapezoidal rule. The discretized problem was coded with the convex optimization tool CVX [14] and solved by the SDPT3 numerical solver for semidefinite-quadratic-linear programming [15]. To improve the numeric efficiency of the tool, the optimization variables b, T_l, T_r, and F_{yv} were normalized by appropriate coefficients so that all problem variables are in a similar order of magnitude.

The trajectory illustrated in Fig. 2 has been chosen for our investigations. It features five straights and four turns with different radiuses. Straights and turns are connected to each other through clothoid transitions, which ensures a continuous yaw rate curve. The trajectory is described in discrete form through a vector of p_X and p_Y coordinates and vehicle course p_ψ for each trajectory point. The distance between subsequent points is 20 m in straights and 2 m in curved sections. This ensures a balance between computational effort and precision of the solution. In addition, a speed limit vector defines the maximum admissible speed for each trajectory point. The start and end speed are set at 0.1 m/s.

The tire force limits $F_{yf,max}$ and $F_{yr,max}$ are calculated by assuming a friction coefficient $\mu = 0.5$ at saturation. Furthermore, the nose gear maximum force is limited at 20 % of the saturation value in order to remain in linear conditions. The limits for each wheel result from the weight distribution according to the distances to the center of gravity:

$$F_{yf,max} = 0.2\frac{b_h}{b_v + b_h} \cdot \mu mg$$

$$F_{yl,max} = F_{yr,max} = \frac{1}{2}\frac{b_v}{b_v + b_h} \cdot \mu mg$$

TABLE I. Parameters of aircraft considered

Parameter	Symbol	Value
Mass	m	67,250 kg
Inertia coeff.	J_z	$3.75 \cdot 10^6$ kg $\cdot$ m^2
Main gear y-distance	a	3.795 m
Main gear x-distance	b_h	2.51 m
Nose gear x-distance	b_f	10.19 m
Maximum nose gear lateral force	F_{yv}	3298.6 N
APU idle fuel flow	c_0	0.02 kg/s
APU fuel flow/power	c_1	$6.95 \cdot 10^{-8}$ kg/(s $\cdot$ W)
Cornering stiffness of nose gear	c_f	$1.49 \cdot 10^5$ N/rad
Cornering stiffness of main gear	c_r	$6.16 \cdot 10^5$ N/rad

where g is the gravity acceleration.

The optimization problem of (33) is solved for a mid-size narrow-body aircraft whose parameters are summarized in Table I. The optimizations results are shown in Fig. 3 and 4. Note that while the optimization algorithm uses T_l and T_r as explained in the previous section, the two linear combinations average torque $T_{avg} = (T_l + T_r)/2$ and differential torque $T_{diff} = T_r - T_l$ are shown in the plots for a better understanding of the results. T_{avg} influences the longitudinal dynamics whereas T_{diff} influences the yaw dynamics.

The results show that because the cost function penalizes positive motor torques, differential moments are only applied when the nose gear lateral force limit is reached. This was never the case for this particular trajectory. Due to the simplification made and unlike the behavior of a real vehicle, the nose gear steering does not cause any additional resistance in the longitudinal motion, thus no additional driving force is needed to keep the same speed while cornering.

By inverting (4), it is possible to check if the resulting steering angle commands δ are realistic. Fig. 5 shows that for the considered case, the steering angle δ is never greater than approximately 0.1 radians = 5.7 degrees in modulus. Also, the steering rate $\dot{\delta}$ is always lower than 0.015 rad/s in modulus, which is known to be compatible with the capabilities of real nose gear steering systems. This result is not surprising since the transitions between straights and corners have been designed smoothly in the trajectory definition.

Additional optimizations have been performed to compare different problem setups. To show the effect of the thermal aspects, two different systems are considered: one without thermal limits and one with limits on the total heating energy in the form of (29). For each system, two optimizations are performed: one for minimum time with the cost function (30) and one for mininum fuel consumption with the cost function (32).

Table II summarizes the fuel consumption and travel time for the four optimizations. It can be seen that for each system considered, the difference between the fuel minimizing and the time minimizing optimization is not large. The difference is even smaller if heat energy limits are used. This is due to the relatively high APU idle consumption, which accounts for most of the fuel consumption and makes the trade-off

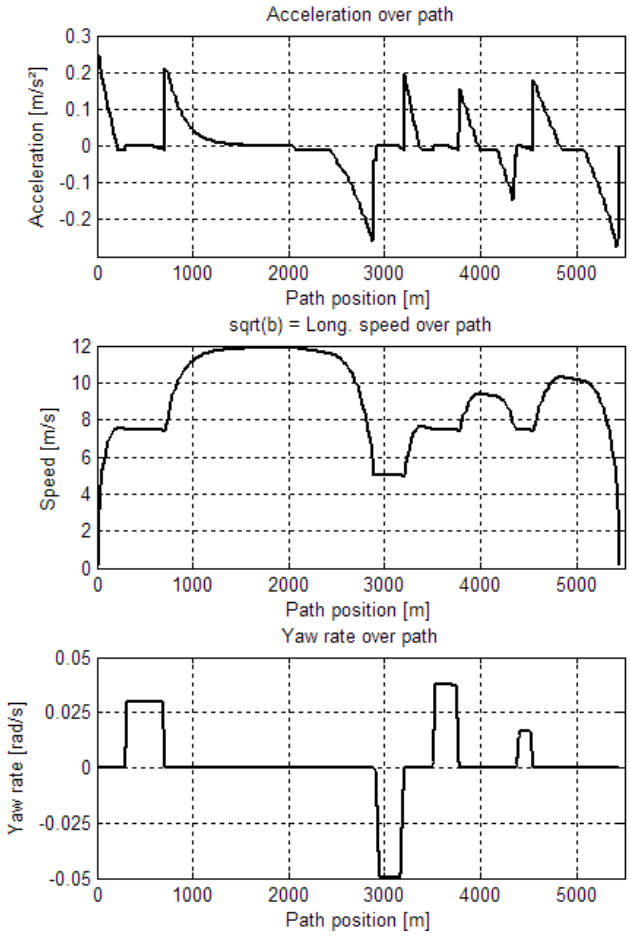

Fig. 3. Optimization results for HC setup, kinematic variables

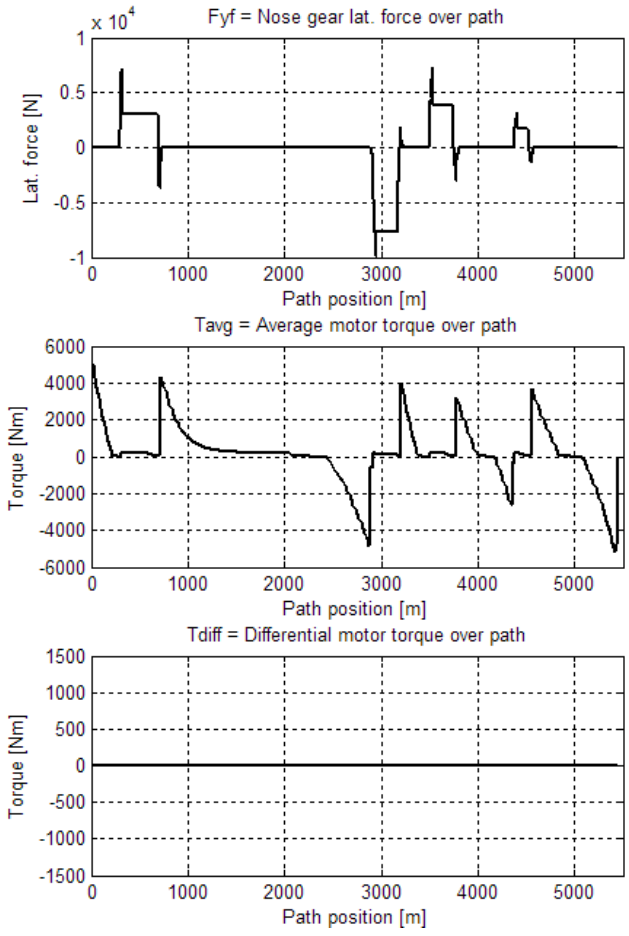

Fig. 4. Optimization results for HC setup, dynamic variables

TABLE II. SUMMARY OF PERFORMED OPTIMIZATIONS WITH MAIN RESULTS

Opt. Name	ϵ	$E_{h,max}$	Time [s]	Fuel Cons. [kg]
T	1	∞	621.3	17.9
C	0	∞	626.1	17.8
HT	1	13	654.3	18.3
HC	0	13	655.9	18.2

between time and fuel consumption notably skewed towards the time minimization. In Fig. 6, the optimizations C and T are compared for the total fuel consumption as well as the two components: idle and driving power. It can be seen that the idle fuel consumption part is much higher than the part pertaining to the driving power in both setups, thus greatly affecting the cost function C_F.

Fig. 7 shows the longitudinal speed profiles of the four optimization setups; for reasons of clarity, only the second half of the trajectory is shown, including the last three corners (nearly constant-speed phases) and the last three straights (accelerating-decelerating peaks). As expected, the time minimizing optimization without thermal limits (optimization T in Fig. 7) commands the highest speeds; the system capabilities are exploited in the straights, with full power either in acceleration or deceleration. In the fuel minimizing optimization without thermal limits (optimization C in Fig. 7), the maximum speeds in straights are lower as driving torques are decreased earlier to save fuel and some kinetic energy is wasted in the rolling phases due to the resistances. The two optimizations with thermal limits (called HT resp. HC in Fig. 7) show a similar pattern. However, the speeds are lower over the whole trajectory compared to the two previous cases because the motor torques are generally kept lower to limit the overall heat energy.

Fig. 8 concentrates on an even smaller part of the trajectory. It shows the nose gear lateral force and the differential torques applied to negotiate the second and the third corner of the trajectory. Here, the time minimizing optimization without thermal limits (T) behaves much differently from the other setups. Since no penalty is imposed on motor torque in the T optimization setup, some differential torques and a lower nose gear lateral force are commanded when cornering. In the other setups, differential torque is penalized either by the cost function itself or indirectly through the heat energy limits, therefore a higher nose gear lateral force is preferred over differential torques.

V. SUMMARY AND OUTLOOK

In the framework of designing electric aircraft taxi systems that allow ground movements without jet engines, this work presented a convex path-following optimization algorithm of

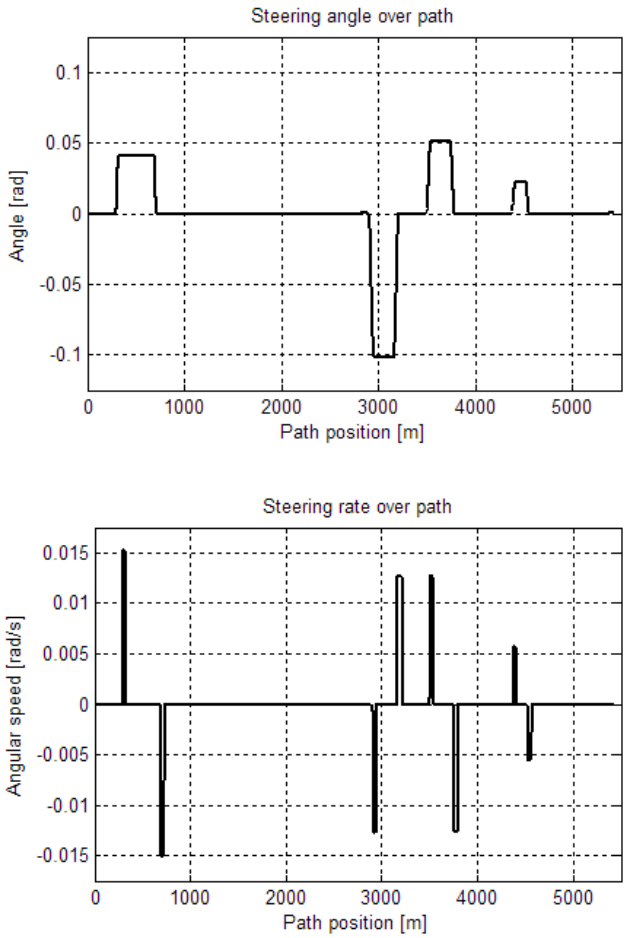

Fig. 5. Optimization results for HC setup, steering angle and steering rate

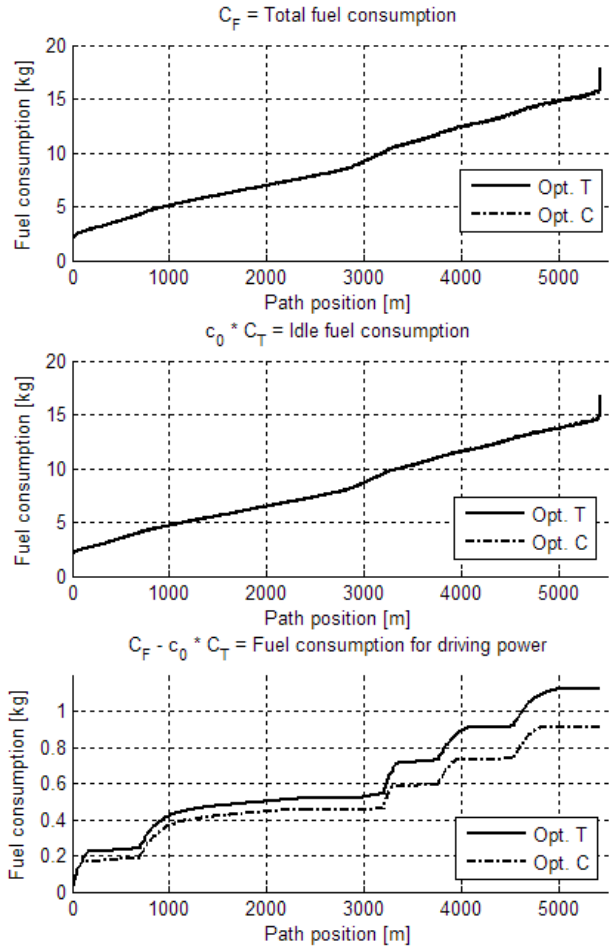

Fig. 6. Comparison between overall fuel consumption as well as idle part and driving power part for the T and C optimization setups

taxi trajectories with a mid-size, narrow-body aircraft equipped with two electric motors on the main landing gears. The convex optimization theory ensure that the solutions are globally optimal for a given system and trajectory. Speed limits and system constraints such as power and heat energy limits have been considered. While different optimization objectives have been tested and compared, the most interesting one is the minimization of the APU fuel consumption during the taxi phase. The results show that the APU idle consumption is a primary driver for this objective.

Future work on this topic will include sensitivity studies to assess the performance variation in dependence of the system parameters. Another interesting development will be to include an energy storage system in the convex problem formulation to allow regenerative braking and evaluate the performance gain in terms of fuel savings and travel time.

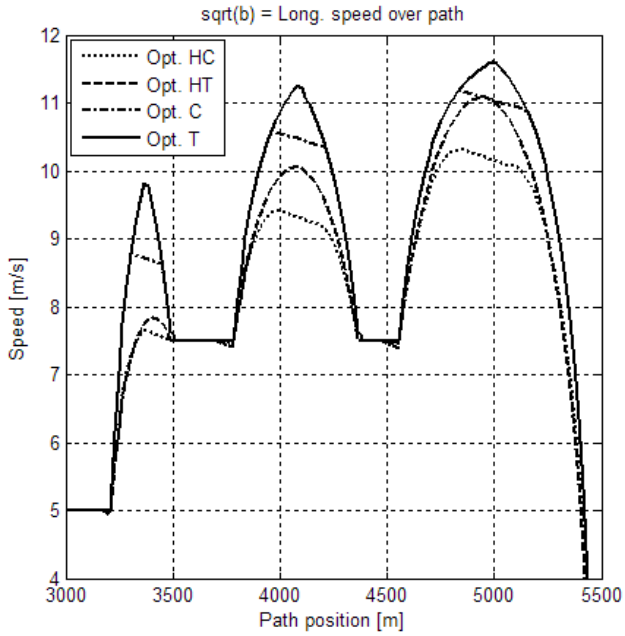

Fig. 7. Comparison between speeds for the four optimization setups in the second part of the test trajectory

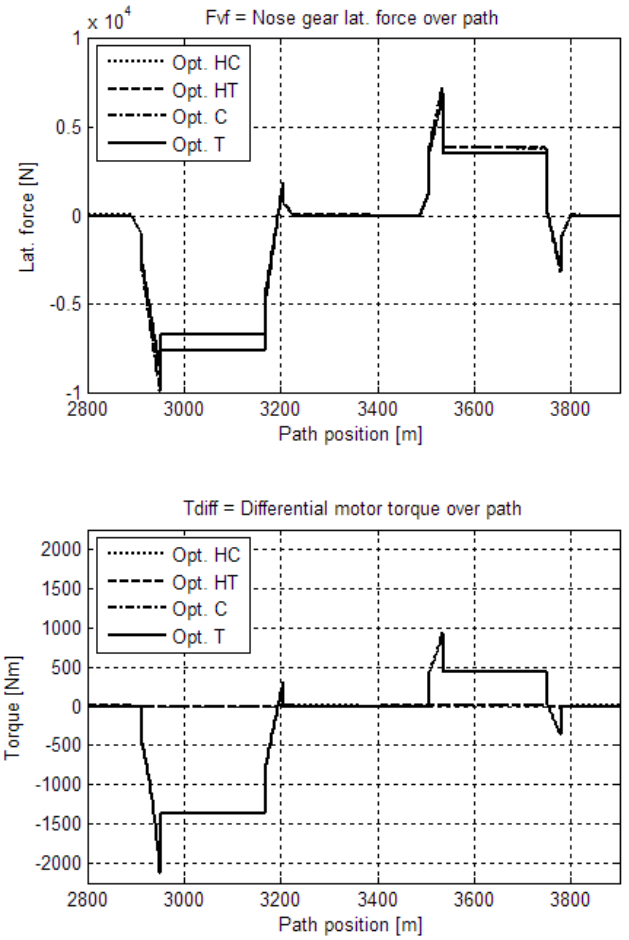

Fig. 8. Comparison between nose gear lateral forces (above) and differential motor torques (below) for the four optimization setups during the second and third corner of the test trajectory

REFERENCES

[1] DLR German Aerospace Center, *DLR Airbus A320 ATRA Taxis Using Fuel-Cell- Powered Nose Wheel for the First Time.* Online: http://www.dlr.de/en/desktopdefault.aspx/tabid-6840/86 read-31408/

[2] Cleansky Joint Technology Initiative Homepage. Online: http://www.cleansky.eu/

[3] Wheeltug Homepage. [Online: http://www.wheeltug.gi/index.shtml

[4] Safran MBD, *Messier-Bugatti's Green Taxing Solutions for Smarter Ground Operations.* Online: http://www.safranmbd.com/actualites/actu-et-communiques-de-presse/article/messier-bugatti-s-green-taxiing?lang=en

[5] Lufthansa Technik, *Joint demonstration of new electric taxi system.* Online: http://www.lufthansa-technik.com/applications/portal/lhtportal/lhtportal.portal?requestednode=395& pageLabel=Template7 8& nfpb=true&webcacheURL=TV I/Media-Relations-new/Press-Releases/E Taxi Demonstration EN.xml

[6] G. Schrmann et al., *The impact of NOx, CO and VOC emissions on the air quality of Zurich airport,* Atmospheric Environment, vol. 41, pp. 103-118, 2007. DOI: 10.1016/j.atmosenv.2006.07.030

[7] F. Re, *Viability and State of the Art of Environmentally Friendly Aircraft Taxiing Systems,* IEEE International Conference on Electrical Systems for Aircraft, Railway and Ship Propulsion ESARS 2012, Bologna, Italy, October 16-18, 2012. DOI 10.1109/ESARS.2012.6387462

[8] S. T. Chai and W. H. Mason, *Landing Gear Integration in Aircraft Conceptual Design*, NASA Ames Research Center & Virginia Polytechnic Institute and State University, Blacksburg, Virginia, September 1996.

[9] F. Re, *Assessing Environmental Benefits of Electric Aircraft Taxiing through Object-Oriented Simulation,* SAE International Journal Aerospace, vol. 5(2), pp. 503-512, 2012. DOI:10.4271/2012-01-2218.

[10] D. Verscheure, B. Demeulenaere, J. Swevers, J. De Schutter, and M. Diehl, *Time-optimal Path Tracking for Robots: a Convex Optimization Approach,* IEEE Transactions on Automatic Control, vol. 54, no. 10, pp. 2318-2327, 2009.

[11] R. de Castro, M. Tanelli, R. E. Arajo, S. M. Savaresi, *Convex Minimum-Time Path Following for Highly Redundant Electric Vehicles*.

[12] S. Boyd and L. Vandenberghe, *Convex Optimization.* Cambridge University Press, 2004.

[13] A. V. Rao, *A survey of numerical methods for optimal control*, in AAS/AIAA Astrodynamics Specialist Conference, 2009.

[14] CVX Research, Inc., "CVX: Matlab software for disciplined convex programming. Version 2.0 beta," 2012.

[15] R. H. Tutuncu, K. C. Toh, and M. J. Todd, "Solving semidefinite-quadratic-linear programs using SDPT3," *Mathematical Programming,* vol. 95, no. 2, pp. 189-217, 2003.
H. Kopka and P. W. Daly, *A Guide to LaTeX*, 3rd ed. Harlow, England: Addison-Wesley, 1999.